THE JOURNAL OF PHYSICAL CHEMISTRY A
A JOURNAL OF THE AMERICAN CHEMICAL SOCIETY

pubs.acs.org/JPCA Article

Photoelectron Spectroscopy and Theoretical Study of Di-Copper–Boron Clusters: $Cu_2B_3^-$ and $Cu_2B_4^-$

Published as part of The Journal of Physical Chemistry A virtual special issue "Krishnan Raghavachari Festschrift".

Anton S. Pozdeev,[⊥] Wei-Jia Chen,[⊥] Hyun Wook Choi, Maksim Kulichenko, Dao-Fu Yuan,* Alexander I. Boldyrev,* and Lai-Sheng Wang*

Cite This: J. Phys. Chem. A 2023, 127, 4888–4896 Read Online

ACCESS | Metrics & More | Article Recommendations | Supporting Information

ABSTRACT: Copper has been found to be able to mediate the formation of bilayer borophenes. Copper–boron binary clusters are ideal model systems to probe the copper–boron interactions, which are essential to understand the growth mechanisms of borophenes on copper substrates. Here, we report a joint photoelectron spectroscopy and theoretical study on two di-copper-doped boron clusters: $Cu_2B_3^-$ and $Cu_2B_4^-$. Well-resolved photoelectron spectra are obtained, revealing the presence of a low-lying isomer in both cases. Theoretical calculations show that the global minimum of $Cu_2B_3^-$ (C_{2v}, $^1A_1$) contains a doubly aromatic B_3^- unit weakly interacting with a Cu_2 dimer, while the low-lying isomer (C_{2v}, $^1A_1$) consists of a B_3 triangle with the two Cu atoms covalently bonded to two B atoms at two vertexes. The global minimum of $Cu_2B_4^-$ (D_{2h}, ^2A_g) is found to consist of a rhombus B_4 unit covalently bonded to the two Cu atoms at two opposite vertexes, whereas in the low-lying isomer (C_s, $^2A'$), one of the two Cu atoms is bonded to two B atoms.

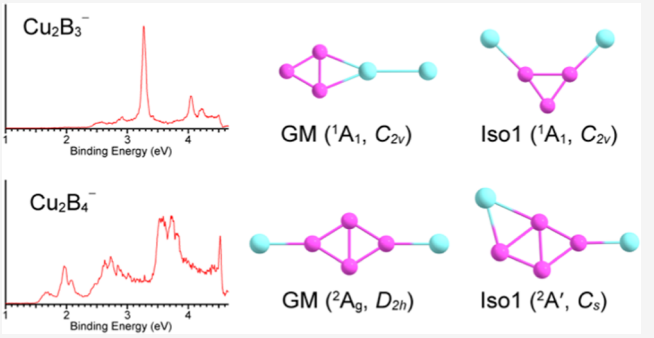

1. INTRODUCTION

The electron deficiency of boron results in the formation of numerous bulk allotropes consisting of different boron cages.[1−3] After the discovery of carbon nanotubes, boron-based nanotubes with a triangular boron layer were proposed.[4,5] However, triangular boron layers are not truly planar and exhibit out-of-plane distortions.[6−9] Theoretical calculations suggested that a triangular boron lattice with hexagonal vacancies could achieve perfect planarity.[10,11] Combined experimental and theoretical studies of size-selected boron clusters provided the first experimental evidence of planarity in small boron clusters.[12−18] Different from bulk boron materials, finite boron clusters have been found to possess two-dimensional (2D) structures consisting of B_3 triangles decorated with vacancies of different shapes and stabilized by delocalized σ and π bonds throughout the cluster plane.[15−17] One of the most important boron clusters is the C_{6v} planar B_{36} cluster that features a central hexagonal hole, providing the first experimental evidence for the viability of monolayer boron sheets, and the name "borophene" was coined for the putative 2D boron nanostructure.[19] Subsequently, borophenes have been successfully synthesized on a variety of inert substrates, becoming a new class of synthetic 2D materials.[20−23] A more recent joint photoelectron spectroscopy (PES) and computational study on B_{48}^- disclosed the first bilayer boron cluster, alluding to the viability of bilayer borophenes.[24] Recently, bilayer borophenes have been successfully synthesized on Cu and Ag substrates.[25,26] Theoretical investigations suggest that electron transfers from the copper substrates to the first boron layer play an important role in the formation of the bilayer borophene.[25] Thus, it is important to study the interaction between copper and boron atoms at the atomic level, in order to understand the growth mechanisms of borophenes on the copper substrate.

There has been a significant amount of work focusing on metal-doped boron clusters to study the interactions between metal atoms and boron motifs via joint experimental and theoretical investigations.[17,27] The study on transition-metal-doped boron clusters revealed a variety of structures including metal-centered molecular wheels,[28−31] metallo-boron nanotubes,[32−34] and metallo-borophenes.[35,36] The closed-shell B_7^{3-},

Received: April 11, 2023
Revised: May 14, 2023
Published: May 26, 2023

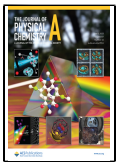

https://doi.org/10.1021/acs.jpca.3c02417
J. Phys. Chem. A 2023, 127, 4888–4896

B_8^{2-}, and B_9^- were found to be σ and π doubly aromatic during the study on small boron clusters,[37,38] and the similarity between their π bonding and that in prototypical hydrocarbons, $C_5H_5^-$, C_6H_6, and $C_7H_7^+$, was recognized in a recent study on LnB_8^- (Ln = La, Pr, Tb, Tm, Yb) clusters.[39] The name "borozene" was proposed for these boron motifs to highlight their aromaticity. Among the three borozenes, B_7^{3-} and B_8^{2-} were realized in multiple metal-doped clusters,[40−45] even in a boron oxide cluster,[46] where the double aromaticity of the borozenes plays an important role in stabilizing the metal-doped boron structures.

Our recent study on $Cu_2B_8^-$ revealed a Cu_2^+−borozene complex,[45] where the charge transfer from copper atoms to the boron motif is similar to what was suggested during the growth of bilayer borophenes on a copper substrate.[25] To further investigate the interaction between copper and boron at the atomic level, we have conducted a joint PES and quantum chemical study on the $Cu_2B_x^-$ (x = 3, 4) clusters. The photoelectron spectra of both clusters are observed to contain contributions from two isomers, as borne out from our global minimum searches. The global minimum of $Cu_2B_3^-$ consists of a B_3^- triangle interacting with a Cu_2 dimer, while a low-lying isomer is found to contain two Cu atoms bonded to two vertexes of a B_3 triangle. The two lowest-energy isomers of $Cu_2B_4^-$ are found to consist of a rhombus B_4 interacting with two separate Cu atoms in different fashions. In the global minimum, the two Cu atoms are bonded to two opposite vertexes, whereas in the low-lying isomer, one of the Cu atoms is bonded to two B atoms. The global minimum of $Cu_2B_3^-$ is dictated by the high stability of the doubly aromatic B_3^- unit, whereas that of $Cu_2B_4^-$ is dominated by the Cu−B covalent bonding.

2. METHODS

2.1. Experimental Method. The experiments were carried out using a PES apparatus consisting of a laser vaporization cluster source, a time-of-flight (TOF) mass spectrometer, and a magnetic bottle photoelectron analyzer, details of which can be found elsewhere.[16,47] The $Cu_2B_x^-$ (x = 3, 4) clusters were produced by laser vaporization of a Cu/^{11}B disk target, compressed from a natural isotope Cu powder and a ^{11}B-enriched (97%) boron powder. The laser-induced plasma was quenched by a pulsed helium carrier gas seeded with 5% argon. Clusters formed in the nozzle were entrained by the carrier gas and underwent a supersonic expansion. After passing a skimmer, anions from the collimated cluster beam were extracted perpendicularly into a TOF mass spectrometer. The clusters of interests were mass-selected and decelerated before interacting with the detachment laser. Two different photon energies from a Nd:YAG laser, 355 nm (3.496 eV) and 266 nm (4.661 eV), were used in the current study. Photoelectrons were collected by the magnetic bottle and analyzed using a 3.5-m-long electron flight tube. The photoelectron kinetic energies were calibrated using the known transitions of the Bi^- atomic anion. The kinetic energy (E_k) resolution ($\Delta E_k/E_k$) of our magnetic bottle photoelectron analyzer was around 2.5%, i.e., ∼25 meV for electrons with 1 eV kinetic energy.

2.2. Theoretical Method. Global minimum (GM) searches were performed using the AFFCK algorithm.[48] At least a thousand random structures were generated for $Cu_2B_3^-$ (singlet and triplet states) and $Cu_2B_4^-$ (doublet and quartet states) during the GM searches. After the initial optimization at the PBE0/LANL2DZ level of theory,[49−51] we reoptimized the low-lying isomers and calculated the harmonic frequencies at the PBE0/aug-cc-pVTZ level of theory.[52,53] We chose the PBE0 functional for its good applicability for boron clusters and their derivatives.[17,54] Then, single point energies for isomers within 15 kcal/mol of the lowest-energy structure were calculated at the CCSD(T)/aug-cc-pVTZ level of theory, which provided more accurate energetic ordering of the isomers. This calculation scheme is denoted as "CCSD(T)/aug-cc-pVTZ//PBE0/aug-cc-pVTZ", but for simplicity, we refer it as CCSD(T) in the text below. We check the convergence of a wavefunction to its ground electronic state using wavefunction test stability.[55] All calculations were performed using the Gaussian-16 software.[56]

The first vertical detachment energy (VDE_1) was calculated as the energy difference between the anion and the corresponding neutral structure at the geometry of the anion. The adiabatic detachment energy (ADE) was calculated as the energy difference between the anion and the corresponding neutral isomer reoptimized after the electron detachment. This approach complies with the fact that photodetachment is a vertical process, i.e., the experimental ADE corresponds to the neutral minimum closest to the anion structure. The ADE and VDEs were calculated by using three approaches: (1) time-dependent DFT (TD-DFT) at the PBE0/aug-cc-pVTZ level, (2) TD-DFT at the CAM-B3LYP/def2-QZVP level,[57,58] and (3) the more accurate ΔCCSD(T)/aug-cc-pVTZ level. For the CAM-B3LYP calculations, VDE_1 calculated at the ΔCCSD(T)/aug-cc-pVTZ level was used as a reference point. We did not include spin−orbit effects in these calculations explicitly in the present work, due to the good agreement between the theoretical VDEs with the experimental data, suggesting that the spin−orbit effects are small. Moreover, the current approach was found to be appropriate in previous studies for similar systems.[43,45] The ORCA 5.03 suite was utilized for the CAM-B3LYP calculations.[59,60]

We performed chemical bonding analyses using the adaptive natural density portioning (AdNDP) method,[61,62] which is a time-proven approach for deciphering delocalized bonding in boron clusters.[15,17,30] It recovers the classical Lewis bonding pictures, i.e., 1-center 2-electron (1c−2e) lone pairs and 2-center 2-electron (2c−2e) bonds and multicenter delocalized bonds (mc-2e bonds, m > 2) and naturally introduces the concepts of aromaticity and antiaromaticity.[63] The AdNDP analyses were done at the PBE0/aug-cc-pVTZ level of theory.

3. EXPERIMENTAL RESULTS

The photoelectron spectra of $Cu_2B_x^-$ (x = 3, 4) at two different wavelengths are presented in Figures 1 and 2 for x = 3 and 4, respectively. The observed PES bands are labeled with letters, and the measured VDEs are given in Tables 1 and 2 for x = 3 and 4, respectively. The ADEs are determined by drawing a straight line at the leading edge of the ground-state detachment transition and then adding the instrumental resolution. In each spectrum, band X represents the transition from the anionic ground state to the ground state of the corresponding neutral at the geometry of the anion. While bands A, B, ··· refer to transitions from the anionic ground state to excited states of the corresponding neutral species. The letters with a prime (X′, A′, ···) indicate transitions from a low-lying isomer.

3.1. $Cu_2B_3^-$. The 355 nm spectrum of $Cu_2B_3^-$ resolved only one major band X centered at 3.28 eV with an estimated ADE of 3.23 eV (Figure 1a). Two minor features, X′ and A′, were

https://doi.org/10.1021/acs.jpca.3c02417
J. Phys. Chem. A 2023, 127, 4888−4896

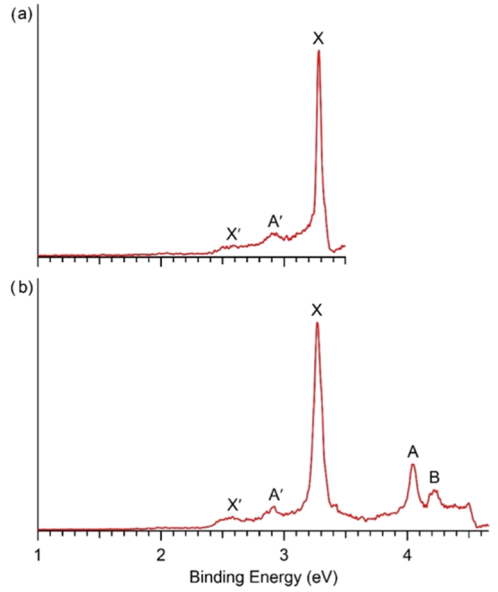

Figure 1. Photoelectron spectra of $Cu_2B_3^-$ at (a) 355 nm (3.496 eV) and (b) 266 nm (4.661 eV).

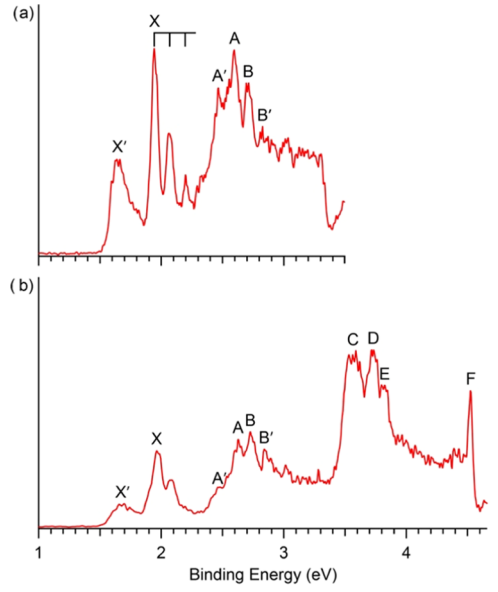

Figure 2. Photoelectron spectra of $Cu_2B_4^-$ at (a) 355 and (b) 266 nm.

observed on the low-binding-energy side at 2.59 and 2.90 eV, respectively, indicating the existence of a possible low-lying isomer. The ADE of band X′ was estimated to be 2.40 eV. At 266 nm (Figure 1b), two new bands at higher binding energies were observed, following an energy gap of ~0.8 eV from band X: band A at 4.04 eV and band B at 4.22 eV. The measured VDEs are given in Table 1, where they are compared with theoretical results (vide infra).

3.2. $Cu_2B_4^-$. The PES features of $Cu_2B_4^-$ are much more complicated than those of $Cu_2B_3^-$. At 355 nm (Figure 2a), the lowest-binding-energy band X′ gives a VDE of 1.64 eV and an estimated ADE of 1.58 eV. Band X is observed to contain a short vibrational progression with a frequency of 1050 (80) cm^{-1}. Both the ADE and VDE of band X are defined by the first intense peak, i.e., the 0−0 transition at 1.94 eV. The PES features from 2.3 to 3.4 eV are quite congested, likely consisting of various electronic and vibrational transitions. Four detachment channels, A′, A, B, and B′ with VDEs of 2.46, 2.60, 2.71, and 2.83 eV, respectively, are tentatively identified. In the 266 nm spectrum (Figure 2b), three more closely spaced features C, D, and E at 3.58, 3.72, and 3.82 eV, respectively, are observed. Finally, a sharp peak *F* is observed near the threshold at 4.52 eV, which is likely the onset of an electronic transition. The measured VDEs are given in Table 2, where they are compared with theoretical results.

4. THEORETICAL RESULTS

The GM structures and low-lying isomers of $Cu_2B_3^-$ and $Cu_2B_4^-$ are shown in Figure 3, arranged according to the relative energies at the CCSD(T) level. More low-lying structures are given Figures S1 and S2 in the Supporting Information. The experimental VDE_1 and ADE are compared with the calculated values for the GM and the lowest-lying isomer for both clusters in Table 3.

4.1. $Cu_2B_3^-$. The three low-lying isomers for $Cu_2B_3^-$ (Figure 3a) are all planar with the GM and Iso1 being almost degenerate at the CCSD(T) level. All of the three low-lying isomers of $Cu_2B_3^-$ consist of a triangular B_3 framework with the two Cu atoms bonded on its periphery in different fashions. The GM has C_{2v} ($^1A_1$) symmetry, where one end of a Cu_2 dimer brides one side of the B_3 triangle. The calculated highest occupied molecular orbital (HOMO)−lowest unoccupied molecular orbital (LUMO) gap is 2.56 eV at the PBE0/aug-cc-pVTZ level, indicating the high electronic stability of the GM structure. In the first low-lying isomer (Iso1 in Figure 3a), the two Cu atoms are bonded to two vertices of the B_3 motif without any Cu−Cu interaction. Although the total

Table 1. Measured VDEs for $Cu_2B_3^-$ Compared with Theoretical Results of the GM and Iso1 at the PBE0/aug-cc-pVTZ and CCSD(T)/aug-cc-pVTZ Levels of Theory (Figure 3a)[a]

	final state and electron configuration	VDE (exp)[b]	VDE (PBE0)	VDE (CCSD(T))
GM (C_{2v}, $^1A_1$)				
X	$^2A_1\{\cdots(5b_2)^2(2a_2)^2(10a_1)^2(5b_1)^2(11a_1)^2(\mathbf{12a_1})^1\}$	3.28	2.89	3.20
A	$^2A_1\{\cdots(5b_2)^2(2a_2)^2(10a_1)^2(5b_1)^2(\mathbf{11a_1})^1(12a_1)^2\}$	4.04	3.88	
B	$^2B_1\{\cdots(5b_2)^2(2a_2)^2(10a_1)^2(\mathbf{5b_1})^1(11a_1)^2(12a_1)^2\}$	4.22	4.06	4.32
Iso1 (C_{2v}, $^1A_1$)				
X′	$^2B_2\{\cdots(3a_2)^2(6b_2)^2(7b_2)^2(8a_1)^2(9a_1)^2(4b_1)^2(\mathbf{8b_2})^1\}$	2.59	2.32	2.45
A′	$^2B_1\{\cdots(3a_2)^2\ (6b_2)^2(7b_2)^2(8a_1)^2(9a_1)^2(\mathbf{4b_1})^1(8b_2)^2\}$	2.90	2.67	2.89
	$^2A_1\{\cdots(3a_2)^2(6b_2)^2(7b_2)^2(8a_1)^2(\mathbf{9a_1})^1(4b_1)^2(8b_2)^2\}$		3.05	3.26
	$^2A_1\{\cdots(3a_2)^2(6b_2)^2(7b_2)^2(\mathbf{8a_1})^1(9a_1)^2(4b_1)^2(8b_2)^2\}$		4.40	

[a]All energies are in eV. [b]The uncertainty of the measured VDEs was 0.02 eV.

https://doi.org/10.1021/acs.jpca.3c02417
J. Phys. Chem. A 2023, 127, 4888−4896

Table 2. Measured VDEs of $Cu_2B_4^-$ Compared with Theoretical Results of the GM and Iso1 at the PBE0/aug-cc-pVTZ and CCSD(T)/aug-cc-pVTZ Levels of Theory (Figure 3b)[a]

	final state and electron configuration	VDE (exp)[b]	VDE (PBE0)	VDE (CCSD(T))
GM (D_{2h}, ^2A_g)				
X	$^1A_g\{\cdots(3b_{2u})^2(6a_g)^2(3b_{3u})^2(6b_{1u})^2(3b_{3g})^2(\mathbf{7a_g})^0\}$	1.94	1.92	1.85
A	$^3B_{3g}\{\cdots(3b_{2u})^2(6a_g)^2(3b_{3u})^2(6b_{1u})^2(\mathbf{3b_{3g}})^1(7a_g)^1\}$	2.60	2.66	2.62
B	$^1B_{3g}\{\cdots(3b_{2u})^2(6a_g)^2(3b_{3u})^2(6b_{1u})^2(\mathbf{3b_{3g}})^1(7a_g)^1\}$	2.71	3.17	2.80
C	$^3B_{1u}\{\cdots(3b_{2u})^2(6a_g)^2(3b_{3u})^2(\mathbf{6b_{1u}})^1(3b_{3g})^2(7a_g)^1\}$	3.58	3.25	3.44
	$^1B_{1u}\{\cdots(3b_{2u})^2(6a_g)^2(3b_{3u})^2(\mathbf{6b_{1u}})^1(3b_{3g})^2(7a_g)^1\}$		3.57	3.55
D	$^3B_{3u}\{\cdots(3b_{2u})^2(6a_g)^2(\mathbf{3b_{3u}})^1(6b_{1u})^2(3b_{3g})^2(7a_g)^1\}$	3.72	3.69	3.67
E	$^1B_{3u}\{\cdots(3b_{2u})^2(6a_g)^2(\mathbf{3b_{3u}})^1(6b_{1u})^2(3b_{3g})^2(7a_g)^1\}$	3.82	4.02	3.85
F	$^3A_g\{\cdots(3b_{2u})^2(\mathbf{6a_g})^1(3b_{3u})^2(6b_{1u})^2(3b_{3g})^2(7a_g)^1\}$	4.52	4.25	4.63
Iso1 (C_s, $^2A'$)				
X′	$^1A'_1\{\cdots(6a'')^2(17a')^2(7a'')^2(18a')^2(19a')^2(\mathbf{20a'})^0\}$	1.64	1.98	1.77
A′	$^3A'_1\{\cdots(6a'')^2(17a')^2(7a'')^2(18a')^2(\mathbf{19a'})^1(20a')^1\}$	2.46	2.04	2.17
B′	$^1A'_1\{\cdots(6a'')^2(17a')^2(7a'')^2(18a')^2(\mathbf{19a'})^1(20a')^1\}$	2.83	2.82	
	$^3A'_1\{\cdots(6a'')^2(17a')^2(7a'')^2(\mathbf{18a'})^1(19a')^2(20a')^1\}$		3.30	
	$^1A'_1\{\cdots(6a'')^2(18a')^2(7a'')^2(\mathbf{18a'})^1(19a')^2(20a')^1\}$		3.61	
	$^3A''_1\{\cdots(6a'')^2(17a')^2(\mathbf{7a''})^1(18a')^2(19a')^2(20a')^1\}$		3.71	
	$^1A''_1\{\cdots(6a'')^2(17a')^2(\mathbf{7a''})^1(18a')^2(19a')^2(20a')^1\}$		4.00	
	$^3A'_1\{\cdots(6a'')^2(\mathbf{17a'})^1(7a'')^2(18a')^2(19a')^2(20a')^1\}$		4.62	

[a]All energies are in eV. [b]The uncertainty of the measured VDEs was 0.02 eV.

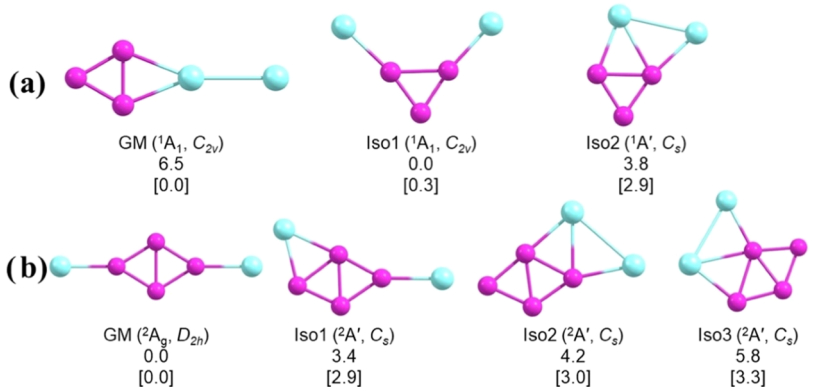

Figure 3. GM structures and low-lying isomers of (a) $Cu_2B_3^-$ and (b) $Cu_2B_4^-$. Relative energies are given in kcal/mol at the PBE0/aug-cc-pVTZ + ZPE level of theory and the CCSD(T)/aug-cc-pVTZ level [in brackets].

Table 3. Experimental ADE and VDE_1 of the GM and the Lowest-Lying Isomer of $Cu_2B_3^-$ and $Cu_2B_4^-$ Compared with Those Calculated at the CCSD(T)/aug-cc-pVTZ Level of Theory[a]

	final state	VDE_1/ADE (exp)[b]	VDE_1/ADE (theor)
$Cu_2B_3^-$ (GM, C_{2v}, $^1A_1$)	$^2A_1$	3.28/3.23	3.20/3.18
$Cu_2B_3^-$ (Iso1, C_{2v}, $^1A_1$)	$^2B_2$	2.59/2.40	2.45/2.21
$Cu_2B_4^-$ (GM, D_{2h}, ^2A_g)	^1A_g	1.94/1.94	1.85/1.83
$Cu_2B_4^-$ (Iso1, C_s, $^2A'$)	$^1A'$	1.64/1.58	1.77/1.72

[a]All energies are in eV. [b]The uncertainty of the measured VDEs was 0.02 eV.

energy of Iso1 (C_{2v},$^1A_1$) is lower than the GM by 6.5 kcal/mol at the PBE0 level, it is only slightly (0.3 kcal/mol) higher than the GM at the CCSD(T) level. Thus, both isomers may exist experimentally. The Iso2 isomer (C_s, $^1A'$) is higher than the GM by 2.9 kcal/mol at the CCSD(T) level. Its structure can be seen as a combination of the GM and Iso1 with one Cu atom bridge-bonded to a B_3 edge and another Cu atom bonded to an adjacent vertex and the first Cu atom. It seems that Cu−Cu interactions are slightly favored over Cu−B interaction in the $Cu_2B_3^-$ cluster.

4.2. $Cu_2B_4^-$. The low-lying isomers of $Cu_2B_4^-$ (Figure 3b) are also planar, all consisting of a B_4 rhombus with the two Cu atoms bonded to its periphery. The GM is a doublet (^2A_g) with D_{2h} symmetry, where the two Cu atoms are bonded to opposite vertices of the B_4 motif. The HOMO−SOMO (β MOs) gap was computed to be 1.2 eV, and the SOMO−LUMO gap (α MOs) was computed to be 3.1 eV, suggesting that the closed-shell D_{2h} $Cu_2B_4^{2-}$ would be a highly stable electronic system. Iso1 with C_s ($^2A'$) symmetry is similar to the GM, except that one of the Cu atoms is shifted from a vertex of the B_4 motif to an edge position. Iso1 is 2.9 kcal/mol higher in energy than the GM at the CCSD(T) level. Both Iso2 (C_s, $^2A'$) and Iso3 (C_s, $^2A'$) involve Cu−Cu interactions with one Cu bonded to an edge position and the other Cu atom bonded to a vertex. At the CCSD(T) level, Iso2 is 3.0 kcal/mol higher in energy than the GM, while Iso3 is 3.3 kcal/mol higher. Apparently, the Cu−B interactions are more important than Cu−Cu interactions in the $Cu_2B_4^-$ cluster.

https://doi.org/10.1021/acs.jpca.3c02417
J. Phys. Chem. A 2023, 127, 4888−4896

5. DISCUSSION

5.1. Comparison between Experiment and Theory and Verification of the Global Minima of $Cu_2B_3^-$ and $Cu_2B_4^-$. Comparison between experiment and theory is essential to verify the GM structures and interpret the photoelectron spectra of $Cu_2B_3^-$ and $Cu_2B_4^-$. The computed VDEs for the GM and the first low-lying isomer for $Cu_2B_3^-$ and $Cu_2B_4^-$ are compared with the experimental data as vertical bars in Figures 4 and 5, respectively. Since the

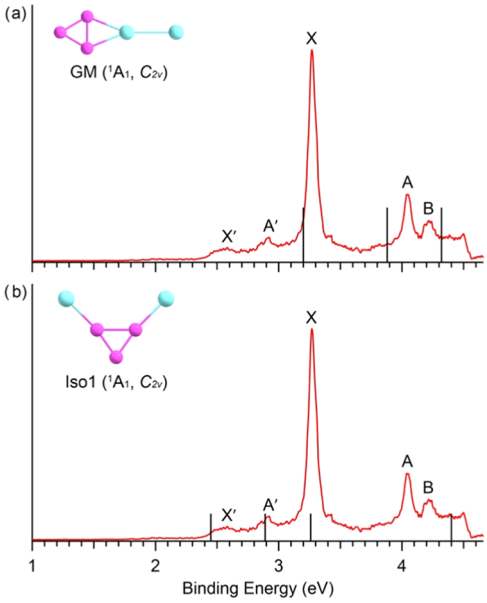

Figure 4. Comparison between the 266 nm photoelectron spectrum and the theoretical results for (a) the GM of $Cu_2B_3^-$ and (b) Iso1 of $Cu_2B_3^-$. The vertical bars correspond to computed VDEs at the CCSD(T)/aug-cc-pVTZ level of theory when available, otherwise at the level of PBE0/aug-cc-pVTZ, as shown in Table 1.

CCSD(T) approach cannot be used to compute every detachment channel due to symmetry constraints (Tables 1 and 2), PBE0 values are also used. We found that the PEB0 VDE values fit the experimental results better than the CAM-B3LYP/def2-QZVP data, which are given in Tables S3 and S4 for the GM structures of $Cu_2B_3^-$ and $Cu_2B_4^-$, respectively. Generally, the closed-shell $Cu_2B_3^-$ structures yield relatively simple spectra (Figure 4), since each fully occupied MO gives only one detachment channel, leading to a doublet final state (Table 1). The $Cu_2B_4^-$ cluster is open shell with an unpaired electron. Therefore, detachment from each fully occupied MO would lead to singlet and triplet final states for both structures (Table 2), resulting in more complicated spectral features (Figure 5).

5.1.1. $Cu_2B_3^-$. The calculated VDE_1 and ADE of the GM and Iso1 of $Cu_2B_3^-$ at the CCSD(T) level are compared with the experimental values in Table 3. The calculated VDE_1/ADE for the C_{2v} GM structure are 3.20/3.18 eV, in good agreement with the experimental values of 3.28/3.23 eV for the observed peak X. On the other hand, the calculated VDE_1/ADE for Iso1 of 2.45/2.21 eV are in good agreement with the experimental values of 2.59/2.40 eV for the weak band X′, providing strong evidence that the weak X′ and A′ bands are due to a low-lying isomer. Since Iso1 is close in energy with the GM at the CCSD(T) level of theory (Figure 3b), it is not surprising that it is populated experimentally.

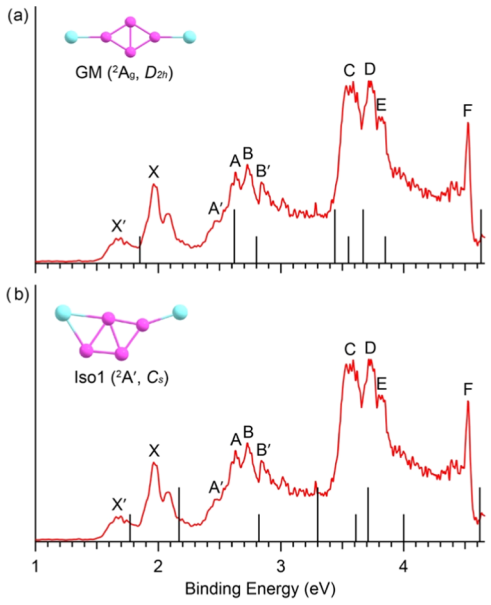

Figure 5. Comparison between the 266 nm photoelectron spectrum and the theoretical results for (a) the GM of $Cu_2B_4^-$ and (b) Iso1 of $Cu_2B_4^-$. The vertical bars correspond to computed VDEs at the CCSD(T)/aug-cc-pVTZ level of theory when available, otherwise at the level of PBE0/aug-cc-pVTZ, as shown in Table 2. The shorter and longer bars correspond to transitions to singlet and triplet final states, respectively.

The first PES band (X) is due to electron detachment from the $12a_1$ HOMO of the GM of $Cu_2B_3^-$, which is primarily a Cu−Cu σ bond (Figure S3). Thus, the strong and sharp X band likely contains a low-frequency Cu−Cu stretching vibrational progression. The HOMO-1 ($11a_1$) of the GM of $Cu_2B_3^-$ has the same symmetry as the HOMO. Thus, its VDE cannot be computed at the CCSD(T) level. The PBE0 VDE value of 3.88 eV is in reasonable agreement with the PES band A at 4.04 eV (Table 1 and Figure 4). The next detachment channel from the HOMO-2 ($5b_1$) gives rise to a VDE of 4.06 eV at the PBE0 level and 4.32 eV at the CCSD(T) level; both are consistent with the observed PES band B at 4.22 eV (Table 1). The HOMO-1 is a delocalized σ orbital and the HOMO-2 is a delocalized π orbital, both on the B_3 unit (Figure S3). The relatively low intensities of bands A and B in comparison to that of band X are consistent with the nature of the MOs because a higher detachment cross section is expected for the Cu-based MO. The excellent agreement between experiment and theory confirms unequivocally the C_{2v} GM structure of $Cu_2B_3^-$ with a Cu−Cu bond.

The weak A′ band at 2.90 eV is in good agreement with the second detachment channel of Iso1 with a computed VDE of 2.89 eV at the CCSD(T) level (Table 1). The computed VDE for the third detachment channel of Iso1 is 3.05 eV at the PBE0 level and 3.26 eV at the CCSD(T) level, which overlaps with band X of the GM. The computed VDE of 4.40 eV for the fourth detachment channel of Iso1 at the PBE0 level is consistent with the weak unresolved signals in the higher-binding-energy side of the 266 nm spectrum (Figure 4). Overall, the combination of the computed VDEs for the GM and Iso1 is in excellent agreement with experimental data (Figure 4), landing considerable credence for the GM of $Cu_2B_3^-$ and the presence of the low-lying isomer.

https://doi.org/10.1021/acs.jpca.3c02417
J. Phys. Chem. A 2023, 127, 4888−4896

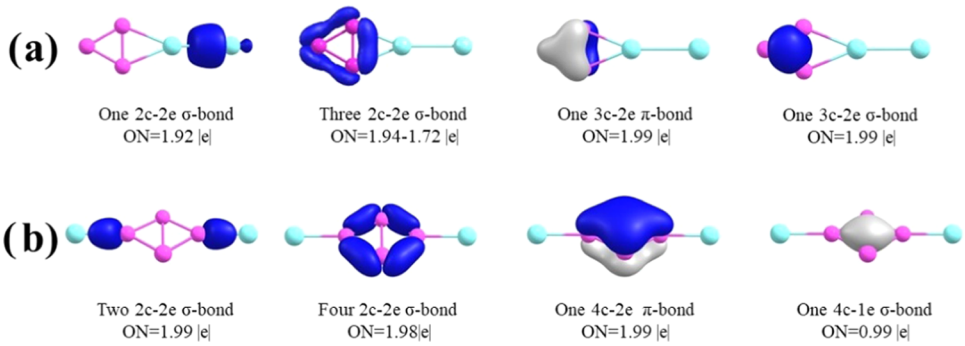

Figure 6. AdNDP bonding analyses for the global minimum structures of (a) $Cu_2B_3^-$ and (b) $Cu_2B_4^-$.

5.1.2. $Cu_2B_4^-$. The calculated VDE_1/ADE for the GM of $Cu_2B_4^-$ are 1.85/1.83 eV at the CCSD(T) level (Table 3), agreeing well with the experimental values of 1.94/1.94 eV. The computed VDE_1/ADE for Iso1 of $Cu_2B_4^-$ is 1.77/1.72 eV, consistent with the experimental VDE/ADE of 1.64/1.58 eV for band X′. These results suggest the presence of Iso1 in the experiment, even though it is 2.9 kcal/mol higher in energy than the GM structure at the CCSD(T) level of theory (Figure 3). We also computed the VDE_1/ADE for Iso2 because it is close in energy to Iso1. Our computed values at the CCSD(T) level are 1.47/1.31 eV, which are too small and do not correspond to any experimental feature. Thus, the presence of Iso2 can be ruled out from the experimental data.

The first PES band (X) for the GM of $Cu_2B_4^-$ is due to the detachment of the electron from the SOMO ($7a_g$), which is a σ bonding orbital involving the two opposite B atoms that are not bonded to Cu (Figure S5). The observed vibrational progression for band X is consistent with the nature of the $7a_g$ orbital. The measured frequency of 1050 ± 80 cm^{-1} is in good agreement with the computed symmetric B−B stretching frequency of 1100 cm^{-1} for neutral Cu_2B_4. The spectral features in the higher binding energy part are congested due to the presence of Iso1 and the fact that detachment from fully occupied MOs from both the GM and Iso1 can produce a triplet and singlet final state. This complication and spectral congestion make it quite challenging to make definitive spectral assignments and quantitative comparison with theory. The assignments given in Table 2 are tentative. However, Figure 5 shows that the computed VDEs for both the GM and Iso1 agree well with the general spectral patterns, providing strong evidence for the D_{2h} GM of $Cu_2B_4^-$ and the presence of the C_s Iso1.

5.2. Chemical Bonding in the Global Minima of $Cu_2B_3^-$ and $Cu_2B_4^-$. We used the AdNDP method to analyze the chemical bonding in the GM structures of $Cu_2B_3^-$ and $Cu_2B_4^-$, as presented in Figure 6. For both anions, we omitted the 10 localized 3d lone pairs (1c−2e) on the Cu atoms. For each 3d lone pair, the ON (occupation number) is in the range of 1.95−2.00|e|, indicating very little participation in bonding.

The AdNDP results for $Cu_2B_3^-$ reveal a 2c−2e Cu−Cu σ bond, three 2c−2e B−B σ-bonds, one 3c−2e π bond, and one 3c−2e σ bond (Figure 6a). It should be noted that the 2c−2e B−B σ-bond next to Cu has a low ON of 1.72, suggesting weak bonding with the Cu atom, whereas the other two 2c−2e B−B σ-bonds have an ON of 1.94. The bonding picture indicates that $Cu_2B_3^-$ can be viewed basically as a Cu_2 dimer weakly interacting with a B_3^-, $[Cu_2][B_3^-]$, in which the B_3^- unit maintains its double aromaticity.[64] In fact, the geometric parameters of B_3^- in the cluster are almost identical to those in the bare B_3^- cluster. The weak B_3^- and Cu_2 interaction is also reflected by the fact that the bond length of the B−B bond (1.537 Å) in contact with Cu is almost the same as the other two B−B bond length (1.534 Å). The high stability of the doubly aromatic B_3^- unit is why the C_{2v} GM structure with the Cu−Cu bond is slightly more stable than Iso1. In Iso1, there are two Cu−B σ bonds, which disrupt the double aromaticity of the B_3^- unit. In fact, the global minimum of $Au_2B_3^-$ is similar to Iso1 of $Cu_2B_3^-$,[65] due to the strong Au−B covalent bonding.[66]

The AdNDP results for $Cu_2B_4^-$ (Figure 6b) display two 2c−2e Cu−B σ bonds, four 2c−2e B−B σ bonds, one 4c−2e π bond, and one 4c−1e σ bond over the B_4 motif. The B_4 unit is one electron short of fulfilling double aromaticity. Thus, it is expected that the rhombus $Cu_2B_4^{2-}$ dianion would be a highly stable chemical species. It is interesting to note that the Cu−B covalent bonding dominates in the GM structure of $Cu_2B_4^-$, similar to Au−B covalent bonding.[65−67] It is expected that as the boron cluster size increases, the Cu−B ionic bonding will be preferred, such as observed in $Cu_2B_8^-$.[45] To find true cluster models to understand Cu−B interactions for the growth of borophenes on copper substrates, it would be interesting to study BCu_x^- or $B_2Cu_x^-$ types of Cu-rich clusters, although Cu-rich boride clusters would be more challenging to produce and separate experimentally due to the natural isotopes of copper. We hope that the current study would stimulate further theoretical investigations.

6. CONCLUSIONS

In conclusion, we report a study of two di-copper-doped boron clusters, $Cu_2B_x^-$ (x = 3, 4), using photoelectron spectroscopy and theoretical calculations. Well-resolved photoelectron spectra are obtained and used to compare with theoretical calculations to understand the structural, electronic, and chemical bonding properties of the two copper boride clusters. The global minimum of $Cu_2B_3^-$ is found to be closed-shell (C_{2v}, $^1A_1$), consisting of a Cu dimer weakly interacting with a doubly aromatic B_3^- motif, whereas a low-lying isomer consisting of a B_3 triangle and two Cu−B bonds is also observed to coexist experimentally. The global minimum of $Cu_2B_4^-$ (D_{2h}, ^2A_g) is found to consist of a rhombus B_4 unit with two Cu−B covalent bonds. A low-lying isomer (C_s, $^2A'$), in which one of the two Cu atoms bonds with two B atoms, is also observed. The high stability of the doubly aromatic B_3^- unit is shown to dictate the global minimum of $Cu_2B_3^-$, while the Cu−B covalent interactions dominate the global minimum of $Cu_2B_4^-$.

https://doi.org/10.1021/acs.jpca.3c02417
J. Phys. Chem. A 2023, 127, 4888−4896

■ ASSOCIATED CONTENT

Supporting Information

The Supporting Information is available free of charge at https://pubs.acs.org/doi/10.1021/acs.jpca.3c02417.

More low-lying structures for $Cu_2B_3^-$ and $Cu_2B_4^-$, valence MO pictures for the GM and the lowest-lying isomers of $Cu_2B_3^-$ and $Cu_2B_4^-$, coordinates of the low-lying isomers of the two clusters, and the computed VDEs at the CAM-B3LYP level of theory for the GM of $Cu_2B_3^-$ and $Cu_2B_4^-$ (PDF)

■ AUTHOR INFORMATION

Corresponding Authors

Dao-Fu Yuan − *Hefei National Research Center for Physical Sciences at the Microscale, University of Science and Technology of China, Hefei 230026, China; Department of Chemistry, Brown University, Providence, Rhode Island 02912, United States*; Email: ydfu@ustc.edu.cn

Alexander I. Boldyrev − *Department of Chemistry and Biochemistry, Utah State University, Logan, Utah 84322, United States*; orcid.org/0000-0002-8277-3669; Email: a.i.boldyrev@usu.edu

Lai-Sheng Wang − *Department of Chemistry, Brown University, Providence, Rhode Island 02912, United States*; orcid.org/0000-0003-1816-5738; Email: lai-sheng_wang@brown.edu

Authors

Anton S. Pozdeev − *Department of Chemistry and Biochemistry, Utah State University, Logan, Utah 84322, United States*

Wei-Jia Chen − *Department of Chemistry, Brown University, Providence, Rhode Island 02912, United States*

Hyun Wook Choi − *Department of Chemistry, Brown University, Providence, Rhode Island 02912, United States*

Maksim Kulichenko − *Theoretical Division, Los Alamos National Laboratory, Los Alamos, New Mexico 87545, United States*; orcid.org/0000-0002-6194-3008

Complete contact information is available at: https://pubs.acs.org/10.1021/acs.jpca.3c02417

Author Contributions

[⊥]W. J. C. and A. S. P. contributed equally to this work.

Notes

The authors declare no competing financial interest.

■ ACKNOWLEDGMENTS

The experiment done at Brown University was supported by the National Science Foundation (CHE-2053541). Computational resources were supported by the Center for High Performance Computing at the University of Utah. M.K. acknowledges support from the Los Alamos National Laboratory (LANL) Directed Research and Development funds.

■ REFERENCES

(1) Albert, B.; Hillebrecht, H. Boron: Elementary challenge for experimenters and theoreticians. *Angew. Chem., Int. Ed.* **2009**, *48*, 8640−8668.

(2) Jemmis, E. D.; Prasad, D. L. V. K. Icosahedral B_{12}, macropolyhedral boranes, β-rhombohedral boron and boron-rich solids. *J. Solid State Chem.* **2006**, *179*, 2768−2774.

(3) Oganov, A. R.; Chen, J.; Gatti, C.; Ma, Y.; Ma, Y.; Glass, C. W.; Liu, Z.; Yu, T.; Kurakevych, O. O.; Solozhenko, V. L. Ionic high-pressure form of elemental boron. *Nature* **2009**, *457*, 863−867.

(4) Gindulytė, A.; Lipscomb, W. N.; Massa, N. L. Proposed boron nanotubes. *Inorg. Chem.* **1998**, *37*, 6544−6545.

(5) Boustani, I.; Quandt, A. Nanotubules of bare boron clusters: Ab initio and density functional study. *Europhys. Lett.* **1997**, *39*, 527.

(6) Boustani, I.; Quandt, A.; Hernandez, E.; Rubio, A. New boron based nanostructured materials. *J. Chem. Phys.* **1999**, *110*, 3176.

(7) Evans, M. H.; Joannopoulos, J. D.; Pantelides, S. T. Electronic and mechanical properties of planar and tubular boron structures. *Phys. Rev. B* **2005**, *72*, No. 045434.

(8) Kunstmann, J.; Quandt, A. Broad boron sheets and boron nanotubes: An ab initio study of structural, electronic, and mechanical properties. *Phys. Rev. B* **2006**, *74*, No. 035413.

(9) Lau, K. C.; Pandey, R. Stability and electronic properties of atomistically-engineered 2D boron sheets. *J. Phys. Chem. C* **2007**, *111*, 2906−2912.

(10) Tang, H.; Ismail-Beigi, S. Novel precursors for boron nanotubes: The competition of two-center and three-center bonding in boron sheets. *Phys. Rev. Lett.* **2007**, *99*, No. 115501.

(11) Yang, X.; Ding, Y.; Ni, J. Ab initio prediction of stable boron sheets and boron nanotubes: Structure, stability, and electronic properties. *Phys. Rev. B* **2008**, *77*, No. 041402.

(12) Zhai, H. J.; Kiran, B.; Li, J.; Wang, L. S. Hydrocarbon analogs of boron clusters: Planarity, aromaticity, and antiaromaticity. *Nat. Mater.* **2003**, *2*, 827−833.

(13) Alexandrova, A. N.; Boldyrev, A. I.; Zhai, H. J.; Wang, L. S. All-boron aromatic clusters as potential new inorganic ligands and building blocks in chemistry. *Coord. Chem. Rev.* **2006**, *250*, 2811−2866.

(14) Oger, E.; Crawford, N. R. M.; Kelting, R.; Weis, P.; Kappes, M. M.; Ahlrichs, R. Boron cluster cations: transition from planar to cylindrical structures. *Angew. Chem., Int. Ed.* **2007**, *46*, 8503−8506.

(15) Sergeeva, A. P.; Popov, I. A.; Piazza, Z. A.; Li, W. L.; Romanescu, C.; Wang, L. S.; Boldyrev, A. I. Understanding boron through size-selected clusters: Structure, chemical bonding, and fluxionality. *Acc. Chem. Res.* **2014**, *47*, 1349−1358.

(16) Wang, L. S. Photoelectron spectroscopy of size-selected boron clusters: from planar structures to borophenes and borospherenes. *Int. Rev. Phys. Chem.* **2016**, *35*, 69−142.

(17) Jian, T.; Chen, X.; Li, S. D.; Boldyrev, A. I.; Li, J.; Wang, L. S. Probing the structures and bonding of size-selected boron and doped-boron clusters. *Chem. Soc. Rev.* **2019**, *48*, 3550−3591.

(18) Pan, S.; Barroso, J.; Jalife, S.; Heine, T.; Asmis, K. R.; Merino, G. Fluxional boron clusters: from theory to reality. *Acc. Chem. Res.* **2019**, *52*, 2732−2744.

(19) Piazza, Z. A.; Hu, H. S.; Li, W. L.; Zhao, Y. F.; Li, J.; Wang, L. S. Planar hexagonal B_{36} as a potential basis for extended single-atom layer boron sheets. *Nat. Commun.* **2014**, *5*, No. 3113.

(20) Mannix, A. J.; Zhou, X. F.; Kiraly, B.; Wood, J. D.; Alducin, D.; Myers, B. D.; Liu, X.; Fisher, B. L.; Santiago, U.; Guest, J. R.; et al. Synthesis of borophenes: Anisotropic, two-dimensional boron polymorphs. *Science* **2015**, *350*, 1513.

(21) Feng, B.; Zhang, J.; Zhong, Q.; Li, W.; Li, S.; Li, H.; Cheng, P.; Meng, S.; Chen, L.; Wu, K. Experimental realization of two-dimensional boron sheets. *Nat. Chem.* **2016**, *8*, 563−568.

(22) Xie, S. Y.; Wang, Y.; Li, X. B. Flat boron: A new cousin of graphene. *Adv. Mater.* **2019**, *31*, No. 1900392.

(23) Kaneti, Y. V.; Benu, D. P.; Xu, X.; Yuliarto, B.; Yamauchi, Y.; Golberg, D. Borophene: Two-dimensional boron monlayer: Synthsis, properties, and potenital applications. *Chem. Rev.* **2022**, *122*, 1000−1051.

(24) Chen, W. J.; Ma, Y. Y.; Chen, T. T.; Ao, M. Z.; Yuan, D. F.; Chen, Q.; Tian, X. X.; Mu, Y. W.; Li, S. D.; Wang, L. S. B_{48}^-: a bilayer boron cluster. *Nanoscale* **2021**, *13*, 3868−3876.

(25) Chen, C.; Lv, H.; Zhang, P.; Zhuo, Z.; Wang, Y.; Ma, C.; Li, W.; Wang, X.; Feng, B.; Cheng, P.; et al. Synthesis of bilayer borophene. *Nat. Chem.* **2022**, *14*, 25.

(26) Liu, X.; Li, Q.; Ruan, Q.; Rahn, M. S.; Yakobson, B. I.; Hersam, M. C. Borophene synthesis beyond the single-atomic-layer limit. *Nat. Mater.* **2022**, *21*, 35.
(27) Barroso, J.; Pan, S.; Merino, G. Strucutral transformations in boron clusters induced by metal doping. *Chem. Soc. Rev.* **2022**, *51*, 1098−1123.
(28) Romanescu, C.; Galeev, T. R.; Li, W. L.; Boldyrev, A. I.; Wang, L. S. Aromatic metal-centered monocyclic boron rings: $Co©B_8^-$ and $Ru©B_9^-$. *Angew. Chem., Int. Ed.* **2011**, *50*, 9334−9337.
(29) Galeev, T. R.; Romanescu, C.; Li, W. L.; Wang, L. S.; Boldyrev, A. I. Observation of the highest coordination number in planar species: decacoordinated $Ta©B_{10}^-$ and $Nb©B_{10}^-$ anions. *Angew. Chem., Int. Ed.* **2012**, *51*, 2101−2105.
(30) Romanescu, C.; Galeev, T. R.; Li, W. L.; Boldyrev, A. I.; Wang, L. S. Transition-metal-centered monocyclic boron wheel clusters ($M©B_n$): A new class of aromatic borometallic compounds. *Acc. Chem. Res.* **2013**, *46*, 350−358.
(31) Chen, T. T.; Li, W. L.; Bai, H.; Chen, W. J.; Dong, X. R.; Li, J.; Wang, L. S. $Re©B_8^-$ and $Re©B_9^-$: New members of the transition-metal-centered borometallic molecular wheel family. *J. Phys. Chem. A* **2019**, *123*, 5317−5324.
(32) Popov, I. A.; Jian, T.; Lopez, G. V.; Boldyrev, A. I.; Wang, L. S. Cobalt-centred boron molecular drums with the highest coordination number in the CoB_{16}^- cluster. *Nat. Commun.* **2015**, *6*, No. 8654.
(33) Li, W. L.; Chen, T. T.; Jiang, Z. Y.; Chen, W. J.; Hu, H. S.; Wang, L. S.; Li, J. Probing the electronic structure of the CoB_{16}^- drum complex: The unusual oxidation state of Co(-I). *Chin. J. Chem. Phys.* **2019**, *32*, 241−247.
(34) Li, W. L.; Jian, T.; Chen, X.; Li, H. R.; Chen, T. T.; Luo, X. M.; Li, S. D.; Li, J.; Wang, L. S. Observation of a metal-centered B 2 18−tubular molecular rotor and a perfect 20−boron drum with the record coordination number of twenty. *Chem. Commun.* **2017**, *53*, 1587−1590.
(35) Li, W. L.; Jian, T.; Chen, X.; Chen, T. T.; Lopez, G. V.; Li, J.; Wang, L. S. The planar CoB_{18}^- cluster as a motif for metallo-borophenes. *Angew. Chem., Int. Ed.* **2016**, *55*, 7358−7363.
(36) Li, W. L.; Chen, X.; Jian, T.; Chen, T. T.; Li, J.; Wang, L. S. From planar boron clusters to borophenes and metalloborophenes. *Nat. Rev. Chem.* **2017**, *1*, 0071.
(37) Alexandrova, A. N.; Boldyrev, A. I.; Zhai, H. J.; Wang, L. S. Electronic structure, isomerism, and chemical bonding in B_7^- and B_7. *J. Phys. Chem. A* **2004**, *108*, 3509−3517.
(38) Zhai, H. J.; Alexandrova, A. N.; Birch, K. A.; Boldyrev, A. I.; Wang, L. S. Hepta- and octacoordinated boron in molecular wheels of eight- and nine-atom boron clusters: Observation and confirmation. *Angew. Chem., Int. Ed.* **2003**, *42*, 6004−6008.
(39) Li, W. L.; Chen, T. T.; Chen, W. J.; Li, J.; Wang, L. S. Monovalent lanthanide(I) in borozene complexes. *Nat. Commun.* **2021**, *12*, No. 6467.
(40) Alexandrova, A. N.; Zhai, H. J.; Wang, L. S.; Boldyrev, A. I. Molecular wheel B_8^{2-} as a new inorganic ligand. Photoelectron spectroscopy and *ab initio* characterization of LiB_8^-. *Inorg. Chem.* **2004**, *43*, 3552−3554.
(41) Galeev, T. R.; Romanescu, C.; Li, W. L.; Wang; Boldyrev, A. I. Valence isoelectronic substitution in the B_8^- and B_9^- molecular wheels by an Al dopant atom: Umbrella-like structures of AlB_7^- and AlB_8^-. *J. Chem. Phys.* **2011**, *135*, No. 104301.
(42) Chen, T. T.; Li, W. L.; Jian, T.; Chen, X.; Li, J.; Wang, L. S. PrB_7^-: A praseodymium-doped boron cluster with a Pr^{II} center coordinated by a doubly aromatic planar η^7-B_7^{3-} ligand. *Angew. Chem., Int. Ed.* **2017**, *56*, 6916−6920.
(43) Chen, W. J.; Kulichenko, M.; Choi, H. W.; Cavanagh, J.; Yuan, D. F.; Boldyrev, A. I.; Wang, L. S. Photoelectron spectroscopy of size-selected bismuth-boron clusters: BiB_n^-(n = 6−8). *J. Phys. Chem. A* **2021**, *125*, 6751−6760.
(44) Chen, W. J.; Zhang, Y. Y.; Li, W. L.; Choi, H. W.; Li, J.; Wang, L. S. AuB_8^-: An Au-borozene complex. *Chem. Commun.* **2022**, *58*, 3134−3137.
(45) Kulichenko, M.; Chen, W. J.; Choi, H. W.; Yuan, D. F.; Boldyrev, A. I.; Wang, L. S. Probing copper-boron interactions in the $Cu_2B_8^-$ bimetallic cluster. *J. Vac. Sci. Technol., A* **2022**, *40*, No. 042201.
(46) Tian, W. J.; Chen, W. J.; Yan, M.; Li, R.; Wei, Z. H.; Chen, T. T.; Chen, Q.; Zhai, H. J.; Li, S. D.; Wang, L. S. Transition-metal-like bonding behaviors of a boron atom in a boron-cluster boronyl complex [(η^7-B_7)-B-BO]$^-$. *Chem. Sci.* **2021**, *12*, 8157−8164.
(47) Wang, L. S.; Cheng, H. S.; Fan, J. Photoelectron spectroscopy of size-selected transition metal clusters: Fe_n^-, n = 3−24. *J. Chem. Phys.* **1995**, *102*, 9480−9493.
(48) Zhai, H.; Ha, M. A.; Alexandrova, A. N. AFFCK: Adaptive Force-Field-Assisted *ab Initio* coalescence kick method for global minimum search. *J. Chem. Theory Comput.* **2015**, *11*, 2385−2393.
(49) Adamo, C.; Barone, V. Toward reliable density functional methods without adjustable parameters: The PBE0 model. *J. Chem. Phys.* **1999**, *110*, 6158−6170.
(50) Wadt, W. R.; Hay, P. J. Ab initio effective core potentials for molecular calculations. Potentials for main group elements Na to Bi. *J. Chem. Phys.* **1985**, *82*, 284−298.
(51) Hay, P. J.; Wadt, W. R. *Ab initio* effective core potentials for molecular calculations. Potentials for K to Au including the outermost core orbitals. *J. Chem. Phys.* **1985**, *82*, 299−310.
(52) Dunning, T. H. Gaussian basis sets for use in correlated molecular calculations. I. The atoms boron through neon and hydrogen. *J. Chem. Phys.* **1989**, *90*, 1007−1023.
(53) Balabanov, N. B.; Peterson, K. A. Systematically convergent basis sets for transition metals. I. All-electron correlation consistent basis sets for the 3d elements Sc−Zn. *J. Chem. Phys.* **2005**, *123*, No. 064107.
(54) Jian, T.; Li, W. L.; Popov, I. A.; Lopez, G. V.; Chen, X.; Boldyrev, A. I.; Li, J.; Wang, L. S. Manganese-centered tubular boron cluster − MnB_{16}^-: A new class of transition-metal molecules. *J. Chem. Phys.* **2016**, *144*, No. 154310.
(55) Bauernschmitt, R.; Ahlrichs, R. Stability analysis for solutions of the closed shell Kohn−Sham equation. *J. Chem. Phys.* **1996**, *104*, 9047−9052.
(56) Frisch, M. J.; Trucks, G. W.; Schlegel, H. B.; Scuseria, G. E.; Robb, M. A.; Cheeseman, J. R.; Scalmani, G.; Barone, V.; Petersson, G. A.; Nakatsuji, H.et al. *G16_C01. 2016, Gaussian 16*, Revision C.01; Gaussian, Inc.: Wallin.
(57) Bannwarth, C.; Grimme, S. A simplified time-dependent density functional theory approach for electronic ultraviolet and circular dichroism spectra of very large molecules. *Comput. Theor. Chem.* **2014**, *1040*, 45−53.
(58) Weigend, F.; Ahlrichsb, R. Balanced basis sets of split valence, triple zeta valence and quadruple zeta valence quality for H to Rn: Design and assessment of accuracy. *Phys. Chem. Chem. Phys.* **2005**, *7*, 3297.
(59) Neese, F. The ORCA program system. *Wiley Interdiscip. Rev.: Comput. Mol. Sci.* **2012**, *2*, 73−78.
(60) Neese, F. Software update: The ORCA program system—Version 5.0. *Wiley Interdiscip. Rev.: Comput. Mol. Sci.* **2022**, *12*, No. e1606.
(61) Zubarev, D. Y.; Boldyrev, A. I. Developing paradigms of chemical bonding: adaptive natural density partitioning. *Phys. Chem. Chem. Phys.* **2008**, *10*, 5207−5217.
(62) Tkachenko, N. V.; Boldyrev, A. I. Chemical bonding analysis of excited states using the adaptive natural density partitioning method. *Phys. Chem. Chem. Phys.* **2019**, *21*, 9590−9596.
(63) Boldyrev, A. I.; Wang, L. S. All-metal aromaticity and antiaromaticity. *Chem. Rev.* **2005**, *105*, 3716−3757.
(64) Zhai, H. J.; Wang, L. S.; Alexandrova, A. N.; Boldyrev, A. I.; Zakrzewski, V. G. Photoelectron spectroscopy and ab initio study of B_3^- and B_4^- anions and their neutrals. *J. Phys. Chem. A* **2003**, *107*, 9319−9328.
(65) Chen, Q.; Bai, H.; Zhai, H. J.; Li, S. D.; Wang, L. S. Photoelectron spectroscopy of boron-gold alloy clusters and boron

https://doi.org/10.1021/acs.jpca.3c02417
J. Phys. Chem. A 2023, 127, 4888−4896

boronyl clusters: $B_3Au_n^-$ and $B_3(BO)_n^-$ (n = 1, 2). *J. Chem. Phys.* **2013**, *139*, No. 044308.
(66) Wang, L. S. Covalent gold. *Phys. Chem. Chem. Phys.* **2010**, *12*, 8694−8705.
(67) Zhai, H. J.; Wang, L. S.; Zubarev, D. Y.; Boldyrev, A. I. Gold apes hydrogen. The structure and bonding in the planar $B_7Au_2^-$ and B_7Au_2 clusters. *J. Phys. Chem. A* **2006**, *110*, 1689−1693.

https://doi.org/10.1021/acs.jpca.3c02417
J. Phys. Chem. A 2023, 127, 4888−4896